High-Flux X-Ray Emission due to Injection into a Laser-Wakefield Accelerator beyond Its Depletion Length

J. C. Wood,[1,*] K. Põder,[1] N. C. Lopes,[1,2] J. M. Cole,[1] S. Alatabi,[1] A. J. Hughes,[1] P. Foster,[3] C. Kamperidis,[1] O. Kononenko,[4] S. P. D. Mangles,[1] D. Neely,[3,†] C. A. J. Palmer,[4] D. R. Rusby,[3] G. Sarri,[5] M. J. V. Streeter,[1] D. R. Symes,[3] J. R. Warwick,[5] and Z. Najmudin[1,‡]

[1]*The John Adams Institute for Accelerator Science, Imperial College London, London SW7 2AZ, United Kingdom*
[2]*GoLP/Instituto de Plasmas e Fusão Nuclear, Instituto Superior Técnico, U.L., Lisboa 1049-001, Portugal*
[3]*Central Laser Facility, STFC Rutherford Appleton Laboratory, Didcot OX11 0QX, United Kingdom*
[4]*Deutsches Elektronen-Synchrotron DESY, Notkestrasse 85, 22607 Hamburg, Germany*
[5]*Queen's University Belfast, University Road, Belfast BT7 1NN, United Kingdom*

(Received 13 September 2024; accepted 9 July 2026; published 3 September 2026)

Laser wakefield accelerators are bright, compact sources of synchrotronlike x-rays. By driving the wakefield using a 110 TW laser in a variable length gas cell, we are able to map the evolution of the electron beam and resulting x-ray emission. We find that using a laser pulse initially focused to larger than the matched spot size and extending the plasma length beyond the depletion length, dramatically increases the x-ray flux. Self-injected electrons are initially accelerated to > 2 GeV, emitting x-rays with critical energy $E_c > 20$ keV. But, as these electrons dephase, a second high-charge electron bunch is produced and accelerated to ≈ 0.7 GeV. The x-rays produced by this bunch dominate the total emission with $> 5 \times 10^{10}$ photons per shot with $E_c = 12$–17 keV and a flux of 7×10^4 photons/mrad^2/0.1%BW. Combining electron and x-ray measurements reveals that the increased emission results from the larger betatron amplitude of the secondary bunch. Simulations attribute this to rapid bubble expansion driven by laser compression over the depletion length, which leads to injection of a high-charge electron bunch with increased transverse momentum and thus stronger betatron radiation.

DOI: 10.1103/krsl-322s

Bright x-ray sources are a vital diagnostic tool for a wide range of scientific applications. Their high penetration depth enables subsurface imaging, and their short wavelengths means that their diffraction can reveal structure on the order of the atomic spacing in solids. Short-pulse (femtosecond) x-ray pulses are particularly valuable for freeze-frame imaging of phenomena evolving on the timescales of molecular vibrations and lattice motion [1].

Short-pulse, high-intensity lasers are an attractive driver of these x-ray sources. Not only are they compact, but they can also be focused and compressed to micrometer scale in space and time, properties that can be inherited by the x-rays they produce. X-rays can be generated by bremsstrahlung and line emission from laser-heated solids [2–5], high-harmonic generation [6–9], and scattering from relativistic electrons [10–14]. X-rays are also produced by laser wakefield accelerators (LWFA) [15,16]. In LWFA, laser pulses focused to normalized vector potential $a_0 = eA_0/m_e c \gtrsim 2$ in underdense plasma, can generate an almost spherical "bubble" devoid of electrons in the wake of the laser pulse [17,18]. Electrons injected into this wakefield can be accelerated to gigaelectronvolt energies in centimeter distances [19–23]. The wakefield bubble also provides a strong focusing force, causing the accelerated electrons to perform "betatron" oscillations. The wiggling motion produces bright, broadband synchrotronlike x-rays with energies of a few to tens of kiloelectronvolts [24–29]. The high directionality of this betatron emission means that it can outshine other laser-produced sources at large distances.

Owing to the short temporal and spatial scale of the electron bunch that produces it, betatron radiation has micrometer-scale source size [26,30,31] and duration in the tens of femtoseconds [32]. The small source size enables high resolution, lensless absorption and phase-contrast imaging in a compact x-ray beamline, with many applications in biology and industry [28,33–41]. The ultrashort nature of the radiation allows the study of rapidly evolving

*Contact author: jonathan.wood@desy.de
†Deceased.
‡Contact author: z.najmudin@imperial.ac.uk

Published by the American Physical Society under the terms of the Creative Commons Attribution 4.0 International license. Further distribution of this work must maintain attribution to the author(s) and the published article's title, journal citation, and DOI.

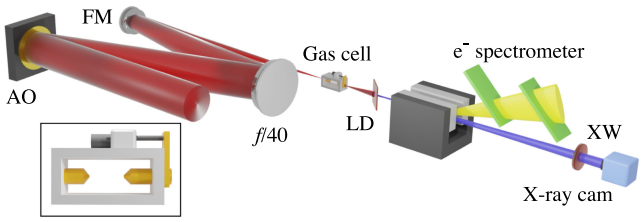


FIG. 1. Experimental setup. The laser (red) wavefront was flattened with an adaptive optic (AO) and focused by an $f/40$ optic in a folded mirror (FM) geometry into the gas cell. A 25 μm Kapton/24 μm Al laser dump (LD) blocked transmitted light. The electron beam (yellow) was deflected by a 0.4 Tm dipole magnet onto two scintillating Lanex screens (e^- spectrometer). X-rays (blue) exited the vacuum chamber through a 250 μm Kapton window (XW) and were detected by an x-ray camera. The inset shows the gas cell: the laser enters and exits via the hollow cones on the left and right. The target length is varied by moving the exit cone with the linear motor on top.

phenomena such as imaging shock waves [42], or spectroscopy of warm dense matter [43–46].

The high brightness of betatron radiation, presently up to 10^{22}–10^{23} photons/s/mm^2/mrad^2/0.1%BW [26,29], is largely a result of the short pulse length and small source size. For applications such as Laue diffraction [43] and x-ray-absorption spectroscopy [45–47], and to improve the signal to noise of betatron imaging, there is a need to increase the spectral flux F (i.e., photons/mrad^2/0.1%BW). In this Letter, we report on an LWFA generating two populations of electrons: a 2 GeV component producing a harder x-ray pulse and a sub-GeV, larger source size component producing a moderate-energy but exceptionally high-flux burst of x-rays. The spectral flux was up to 10 times higher than other configurations using the same laser system [29,46]. Simulations show that the secondary injection is due to the self-compression of the laser pulse over the depletion length [48] leading to rapid bubble expansion that injects and accelerates electrons with increased transverse momentum.

The experiment was performed using the Gemini laser at the Rutherford-Appleton Laboratory [49]. The setup is shown in Fig. 1. A (5.6 ± 0.3) J, 800 nm laser pulse, slightly positively chirped with duration $\tau = (53 \pm 5)$ fs FWHM, $P \approx 110$ TW, was focused by a 6 m focal length, $f/40$ spherical mirror to the entrance of a helium-filled gas cell. The elliptical $(54 \pm 2) \times (45 \pm 1)$ μm (FWHM) spot contained $(32 \pm 3)\%$ of the laser energy, giving a peak $a_0 = 1.3 \pm 0.1$. A limited additional dataset was taken with a higher laser energy of (10.5 ± 0.2) J and $a_0 = 1.8 \pm 0.1$ ($P \approx 220$ TW). A key feature of the gas cell was that its length could be adjusted in the range 3–42 mm, allowing length scans to be performed over a fixed uniform plasma density n_e [50,51]. The plasma density was characterized by moiré interferometry using a transverse probe pulse [52].

A dipole spectrometer measured the energy of the generated electron beam. The use of two scintillating screens allowed pointing uncertainties to be removed via backtracking [53,54]. The low energy cutoff was 230 MeV, and uncertainties were primarily influenced by the positioning of the screens. Absolute charge measurements were obtained by cross-calibration with Imaging Plate [55,56]. The spatial profile of the betatron x-ray beam was measured using an in-vacuum caesium iodide (CsI) scintillator (not shown in Fig. 1). This scintillator could be removed so that the x-rays could exit the vacuum chamber through the Kapton window and be detected by a 150 μm thick CsI scintillator fiber coupled to a CCD camera. The camera had been calibrated for deposited x-ray energy with a Fe-55 radiation source.

The spectrum of the betatron radiation was initially assumed to be an on-axis synchrotron spectrum of the form $S(E, E_c) \propto \gamma^2 (E/E_c)^2 K^2_{2/3}(E/2E_c)$, where E is the photon energy, γ is the electron Lorentz factor, and $K_{2/3}$ is a modified Bessel function of the second kind [26,57,58]. The critical energy $E_c = (3\hbar/4c)\gamma^2 \omega_p^2 r_\beta$, where ω_p is the plasma frequency and r_β is the electron beam oscillation radius. E_c is close to the peak of the intensity curve, and the intensity falls rapidly for $E > 2E_c$. Although the betatron spectrum is more complex [59], a synchrotronlike approximation is commonly used to represent the properties of betatron beams. E_c was obtained from the x-ray transmission through an array of filters placed directly in front of the x-ray detector, as described in the Supplemental Material [60].

A scan of accelerator (gas cell) length, L_a, was performed at $n_e = (2.3 \pm 0.2) \times 10^{18}$ cm^{-3} ($n_{CR}/n_e \approx 750$) and laser energy 5.6 J. Figure 2 shows electron spectra and x-ray filter array images as a function of L_a. An electron beam was observed for $L_a > 3$ mm. Continuous self-injection led to a broad energy spread beam with measured charge (i.e., for $E > 230$ MeV) increasing linearly to $Q = 130$ pC at $L_a = 10$ mm. At this distance, the maximum energy of the bunch is $E_{max} \approx 2$ GeV. Such high energies could only be attained by strong self-focusing and self-compression of the laser pulse, since in the nonlinear regime $E_{max} \approx \frac{2}{3} a_0 (n_{CR}/n_e) m_e c^2$ [48,61]. It has been shown that, approaching the matched spot size from an initially oversized, low a_0 spot, as done here, minimizes the laser spot and thus bubble length oscillations. These would otherwise scatter electrons from the high-field region at the back of the bubble preventing acceleration to the highest energies [54].

Between $L_a = 10$ to 12 mm, a second population of electrons was injected, as seen in Fig. 2. The properties of these electrons are notably different from the first bunch. It contains a greater, more variable charge, $Q = 140$–360 pC, with an average of 4 times more charge per MeV than the first bunch. The two bunches can be differentiated by the large change in spectral density at the maximum energy of the second bunch. This bunch often has a different pointing in the nondispersed direction to the earlier injected electron

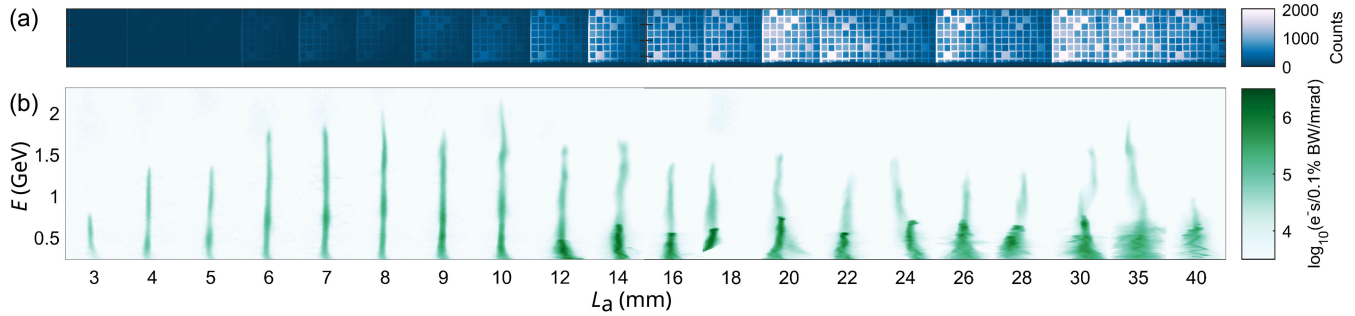


FIG. 2. Experimental data. Representative x-ray camera images of the filter array (a) and their corresponding electron spectra (b) from a plasma length scan. The angular width of each electron spectrum image is 20 mrad.

bunch, which remains as a high energy background extending beyond 1 GeV, even for long L_a. The second bunch, by contrast, does not exceed $E_{\max} = 700$ MeV, as shown in Fig. 3(a). This second bunch is injected at close to the length at which the laser is depleted due to pulse front etching, $L_{\rm pd} = (\omega_0^2/\omega_{\rm p}^2)c\tau = 10.2$ mm, where ω_0 is the laser frequency [48,62]. This secondary injection has been seen before [63], and attributed to the presence of severe longitudinal evolution of the laser pulse [61,64–66].

Figure 2 also shows that the injection and acceleration of the second bunch is associated with a rapid increase in x-ray flux. From $L_{\rm a} = 9$ to 20 mm, the mean recorded x-ray counts increased between sixfold and tenfold. Figure 3(b) plots the variation of $E_{\rm c}^s$, the best-fit critical energy of a synchrotron spectrum assuming a single electron energy γ, with accelerator length, $L_{\rm a}$. For $L_{\rm a} \leq 10$ mm, $E_{\rm c}^s$ increases

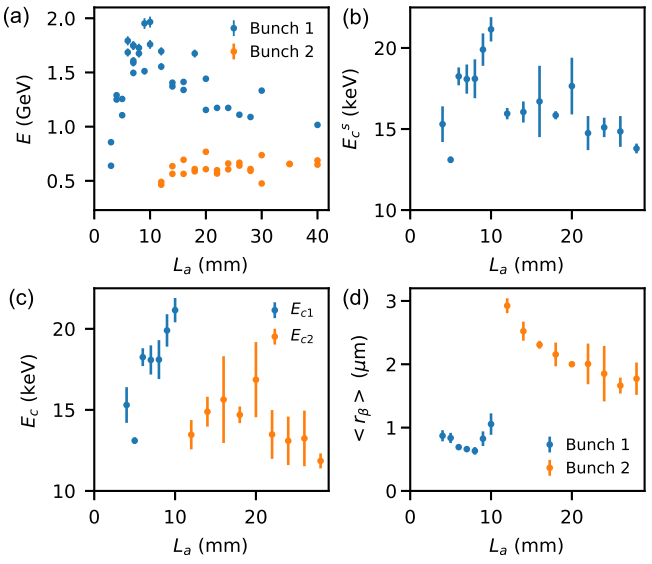


FIG. 3. Variation of electron and x-ray properties with accelerator length, $L_{\rm a}$. (a) Peak electron energies, (b) $E_{\rm c}^s$ assuming a single spectrum fit, (c) $E_{\rm c}$ from a double spectrum fit, (d) $\langle r_\beta \rangle$ of each bunch. The error bars are the standard deviation from multiple shots, except in (a), where they are derived from the uncertainties in the electron beam tracking.

as the first electron bunch is accelerated, as expected from the strong dependence of $E_{\rm c}$ on γ. But at $L_{\rm a} = 12$ mm, $E_{\rm c}^s$ immediately drops from 21 to 16 keV. As the first bunch decelerates, any further radiation it produces would be softer, but this cannot explain such a dramatic decrease in photon energy nor the corresponding increase in photon number. Instead, it suggests that the spectrum becomes dominated by the radiation produced by the second bunch.

To investigate the simultaneous decrease in critical energy and increased photon flux for $L_{\rm a} > L_{\rm pd}$, we consider the cycle-averaged power emitted by each electron, $\langle P \rangle = (e^2 c/12\pi\epsilon_0)\gamma^2\alpha_\beta^2 k_\beta^2$ [67], where the wiggler parameter $\alpha_\beta = \gamma k_\beta r_\beta$, and the wavenumber of the betatron motion $k_\beta = \omega_{\rm p}/(c\sqrt{2\gamma})$. The energy emitted per cycle is $\langle P \rangle \lambda_\beta / c$ where $\lambda_\beta = 2\pi/k_\beta$ is the betatron wavelength. For $N_{\rm e}$ electrons performing N_β oscillations, the total energy emitted is $W_{\rm tot} = (e^2/12\sqrt{2}\epsilon_0 c^3) N_{\rm e} N_\beta \omega_{\rm p}^3 \gamma^{5/2} r_\beta^2$. The greater emission of the second bunch is surprising, considering the strong scaling of $W_{\rm tot}$ with γ, and cannot be explained only by the increased charge of the second bunch, which fluctuated between 1 and 3 times that of the first bunch. This suggests that the second bunch must have a significantly larger oscillation radius than the first.

r_β can be deduced for each bunch from their respective electron and x-ray spectra. Using $r_\beta = r_0 \gamma^{-1/4}$ [68], where r_0 is a constant to be determined for each bunch, then $E_{\rm c} = (3\hbar/4c)\omega_p{}^2 r_0 \langle \gamma^{7/4} \rangle$. Here we average over γ, since the electron beams are broadband. To account for the different properties of the two bunches, we assign a "double" synchrotron spectrum $S_{\rm tot} \propto E^2 K_{2/3}^2(E/2E_{\rm c1}) + RE^2 K_{2/3}^2(E/2E_{\rm c2})$, where R quantifies the relative contribution of each bunch. To reduce the susceptibility of the multiparameter fitting to noise, $E_{\rm c1}$ was held constant at 21.2 keV beyond $L_{\rm a} = 10$ mm, which is its mean value at that point. This assumes that the first bunch did not radiate much after this length, since its peak energy starts to fall. Figure 3(c) plots $E_{\rm c1}$ and $E_{\rm c2}$ versus $L_{\rm a}$, which shows that the second electron bunch produces x-ray radiation with $E_{\rm c} \approx 12$–17 keV. Figure 3(d) is a plot of $\langle r_\beta \rangle = r_0 \langle \gamma^{-1/4} \rangle$ versus $L_{\rm a}$, obtained from the

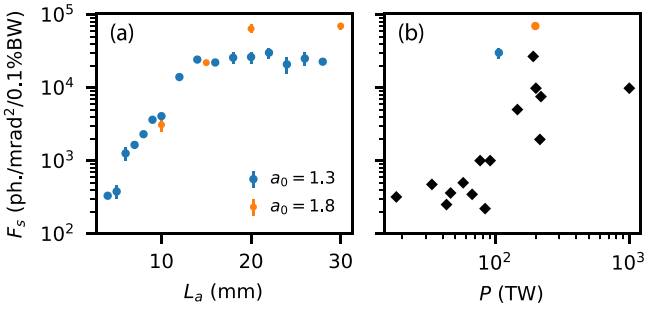


FIG. 4. Measured x-ray spectral flux. (a) F vs L_a for $a_0 = 1.3$ and 1.8. (b) Maximum F as a function of laser power for the $a_0 = 1.3$ and 1.8 data compared to the literature (black diamonds) [21,25,26,29,35,41,46,69–75].

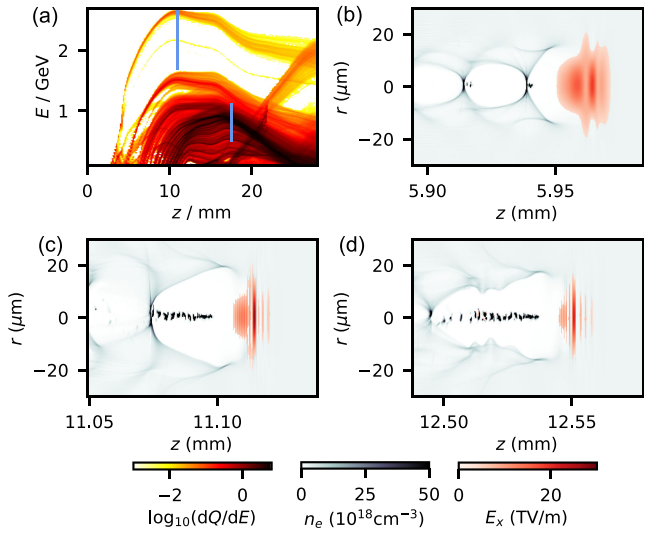


FIG. 5. Simulation results. (a) Evolution of the electron energy spectrum. Vertical lines indicate the z positions and energy ranges used for the emittance analysis in the text. (b)–(d) Maps of plasma density (in the laser polarization plane) and laser electric field envelope for different propagation distances. For clarity, the field is only shown above 4 TV m^{-1}.

simultaneously measured x-ray and electron spectra and the expression for E_c. It shows that the second bunch has a significantly higher r_β of 2–3 μm, compared to 0.6–1 μm for the first bunch. The different scalings of $E_c \propto \gamma^2 r_\beta$ and $W_{tot} \propto \gamma^{5/2} r_\beta^2$ make the emission from the second bunch lower energy but with higher photon number. We also note that the inferred r_β reduces for longer L_a after its rapid increase at $L_a \approx 10$ mm, suggesting that these electrons are injected with a larger oscillation amplitude, rather than it increasing with propagation length.

The peak photon spectral flux F is plotted as a function of L_a in Fig. 4(a). This is obtained by using an array of repeating filters (see the Supplemental Material [60]) to obtain spatially discriminated yield and spectrum. The rapid increase in F between 10 and 15 mm further highlights that most of the x-rays are emitted during the second period of injection. Also plotted in Fig. 4 are data taken with $a_0 = 1.8$ at an optimized density of $n_e = (3.6 \pm 0.4) \times 10^{18}$ cm^{-3}. F follows the same trend, greatly increasing when secondary injection occurs around $L_a = 12$ mm, and its peak is 2.3 times larger than for $a_0 = 1.3$. E_c for these higher power shots was largely independent of L_a at $E_c \approx 20$ keV, with a small reduction to (17.4 ± 0.4) keV at $L_a = 15$ mm, just after the secondary injection. Figure 4(b) plots the maximum F measured here compared to other work as a function of laser power. We see that this is an exceptionally high flux source of betatron radiation, with a maximum value 2.6 times the largest F from other work [46]. In the high a_0 case, with $L_a = 20$ mm, the x-ray beam divergence, linearly extrapolated from data taken at densities of $1.9 - 3.3 \times 10^{18}$ cm^{-3}, was 17×16 mrad FWHM. Taking a 2D Gaussian beam profile with a peak given by the peak photons per pixel on the x-ray CCD, there were a maximum of 5.6×10^{10} photons above 1 keV in the whole x-ray beam. Using a simulated rms pulse length of 42 fs at $L_a = 20$ mm and $r_\beta = 2$ μm, we obtain a peak brightness of 1.3×10^{23}photons/s/mm^2/mrad^2/0.1%BW.

To investigate the injection and acceleration dynamics of the two electron bunches and to better understand the dramatic increase in x-ray yield beyond the dephasing length, quasicylindrical 3D particle-in-cell simulations were run using the code FBPIC [76]. The simulation box was $(120, 120)$ μm in (z, r), with (40, 7.5) cells per micrometer. Two azimuthal modes were used with (2, 2, 6) particles per cell along (z, r, θ). The laser had $a_0 = 1.3$, a FWHM intensity duration of 53 fs, a FWHM width of 49.3 μm (having the same area as the experimental pulse), and was linearly polarized in the x direction. The plasma started with a 0.5 mm linear ramp, up to a uniform density of $n_e = 2.4 \times 10^{18}$ cm^{-3}. The laser was focused at the start of the density plateau.

Figure 5(a) plots the simulated electron spectrum versus propagation distance z. An initial electron bunch was injected at $z = 3$ mm and was accelerated to 2.6 GeV by $z = 12$ mm. This is higher than in the experiment, but is unsurprising given the idealized parameters used in the simulation. As shown in Fig. 5(b), the electron bunch is stably accelerated in a blown-out wakefield. Shortly after the depletion length, $z = 9.8$ mm in the simulation, a dramatic compression of the laser energy is observed [Fig. 5(c)] and a high-amplitude optical shock is formed [77–79]. The rapid increase in a_0 causes the plasma bubble to elongate since its length $\lambda_p \approx 2\pi\sqrt{a_0}c/\omega_p$ [48,66]. This reduces the phase velocity of the wake's accelerating field, which follows the rear of the wake. This in turn reduces the trapping threshold, leading to additional electron injection [61,63–65]. Beam loading due to this secondary injection also contributes to lengthening of the plasma wave [66], leading to an almost continuous injection over an extended length. The continued lengthening of the bubble, shown in

Fig. 5(d), also means these electrons never see the highest fields at the back of the wakefield, and so gain significantly less energy than the first bunch, at most around 1 GeV. For $z > 20$ mm, the laser is no longer sufficiently energetic to drive a wakefield, and a beam-driven regime is entered [80]. This can explain the increase in energy of the first bunch at $L_a \approx 30$–35 mm recorded in the experiment [Fig. 2(c)].

The highest energy electrons from bunches 1 and 2 in the simulation were analyzed at $z = 11$ and 17.5 mm respectively, denoted by the blue lines in Fig. 5(a). These correspond to the points at which the highest density regions of each bunch reach its respective maximum energy, and would thus radiate most strongly. The normalized emittance in x and y were $\epsilon_{N1} = 1.7 \times 0.5$ μm and $\epsilon_{N2} = 2.7 \times 1.6$ μm for bunches 1 and 2. The larger emittance leads to larger oscillation radii since the focusing force of a blown-out wakefield is linear in r and non-evolving. For bunch 1, the emittance in both axes was constant from $z = 5$–20 mm, likewise for bunch 2 from $z = 11$–20 mm (see the Supplemental Material [60]), indicating that their emittance is determined at injection.

The greater emittance of bunch 2 is due to the laser evolution. Between $z = 6$ and 11 mm [Figs. 5(b) and 5(c)], the laser $a_0 = eE_{x,\max}/m_e c\omega$, where $E_{x,\max}$ is the peak laser electric field and ω is its local frequency, increases from 5.6 to 8.2 (see the Supplemental Material [60]). This results in a 46% increase in transverse momentum $p_\perp$ for injected electrons due to the conservation of canonical momentum $\mathbf{p} - e\mathbf{A}$. The bubble radius r_b also increases between $z = 6$ and 11 mm, indicating that the sheath electrons, which are injected later, have a larger $p_\perp$. Balancing the laser ponderomotive and the bubble restoring forces gives $k_p r_b \propto \sqrt{a_0}$ [48]. With $p_\perp \propto a_0$, this results in a quadratic scaling of $p_\perp$ with r_b. In the simulation r_b increases from 14.9 μm to 19 μm between $z = 6$ and 11 mm, suggesting a 63% increase in $p_\perp$, which is in line with the observed increase in emittance.

There have been previous reports of x-ray emission from LWFA driven beyond the depletion length [69,74]. In those cases, increased emission was attributed to high energy electrons gaining extra $p_\perp$ due to interactions with the laser pulse [69] or due to hosing [74]. Since γ is unchanged, both mechanisms should result in a hardening of the x-ray emission (increase in E_c), the direct opposite of what we have measured here. Further, interaction of the accelerated electrons with the laser fields should have been readily observed in increased deflection in Fig. 2, since the laser polarization was orthogonal to the dispersion plane of our spectrometer [81]. Owing to the strong optical compression, this signature is not seen for $L_a \approx L_{pd}$. Indeed, Fig. 3(d) suggests that, if anything, there is a reduction in r_β for the distances over which photon flux increases most rapidly ($L_a \approx 10$–20 mm).

Hosinglike behavior is seen for $z \gtrsim 20$ mm in the simulations, and in the experiment for $L_a \gtrsim 26$ mm (Fig. 2). There is also evidence of self-injection caused by transverse oscillations of the back of the bubble driven by the few-cycle compressed pulse at long interaction lengths (see the movie in the Supplemental Material [60]). In the simulations, these oscillations are rapidly damped, so while they may contribute to an increased $p_\perp$, there is little evidence of large amplitude, coherent betatron oscillations as in [70]. The photons produced by these electrons are of greater divergence ($\theta \approx \alpha_\beta/\gamma$) [82], and do not greatly affect the flux in the spectral range of our measurements. Indeed, there is no dramatic increase in measured flux in Fig. 2 for long interaction lengths.

We have observed an order-of-magnitude increase in the spectral flux of betatron radiation at 10–20 keV due to the injection of a larger r_β electron bunch as a result of laser pulse compression. Greater than 5×10^{10} x-ray photons were produced per shot, with $(7.0 \pm 0.8) \times 10^4$ photons/mrad^2/0.1%BW. The source thus offers improved signal to noise for x-ray imaging applications, while barely diminishing the spatial resolution, as demonstrated in [36,39]. It also offers new possibilities in spectroscopic or diffraction studies [43,46]. This work was performed in a target area of floor space 2×7.5 m^2, by a laser system that requires a similar footprint and can now readily be operated at a greater than 1 Hz rate. These results hence promise increased accessibility for laser-based compact synchrotron light sources for a wide range of applications.

Acknowledgments—The authors acknowledge funding from STFC (No. ST/J002062/1, No. ST/P002021/1, No. ST/V001639/1, and No. UKRI1888) and EPSRC (No. EP/N027175/1). We thank the Central Laser Facility staff for their engineering and technical support, and the Imperial College Research Computing Service for access to computational resources.

Data availability—The data that support the findings of this article are available from the authors upon reasonable request.

[1] J. P. Marangos, Phil. Trans. R. Soc. A **377**, 20170481 (2019).
[2] M. D. Perry, J. A. Sefcik, T. Cowan, S. Hatchett, A. Hunt, M. Moran, D. Pennington, R. Snavely, and S. C. Wilks, Rev. Sci. Instrum. **70**, 265 (1999).
[3] C. Reich, P. Gibbon, I. Uschmann, and E. Förster, Phys. Rev. Lett. **84**, 4846 (2000).
[4] R. D. Edwards, M. A. Sinclair, T. J. Goldsack, K. Krushelnick, F. N. Beg, E. L. Clark, A. E. Dangor, Z. Najmudin, M. Tatarakis, B. Walton, M. Zepf, K. W. D. Ledingham, I. Spencer, P. A. Norreys, R. J. Clarke,

R. Kodama, Y. Toyama, and M. Tampo, Appl. Phys. Lett. **80**, 2129 (2002).
[5] C. M. Brenner, S. R. Mirfayzi, D. R. Rusby, C. Armstrong, A. Alejo, L. A. Wilson, R. Clarke, H. Ahmed, N. M. H. Butler, D. Haddock, A. Higginson, A. McClymont, C. Murphy, M. Notley, P. Oliver, R. Allott, C. Hernandez-Gomez, S. Kar, P. McKenna, and D. Neely, Plasma Phys. Controlled Fusion **58**, 014039 (2015).
[6] M. Ferray, A. L'Huillier, X. F. Li, L. A. Lompre, G. Mainfray, and C. Manus, J. Phys. B **21**, L31 (1988).
[7] X. F. Li, A. L'Huillier, M. Ferray, L. A. Lompré, and G. Mainfray, Phys. Rev. A **39**, 5751 (1989).
[8] J. Seres, E. Seres, A. J. Verhoef, G. Tempea, C. Streli, P. Wobrauschek, V. Yakovlev, A. Scrinzi, C. Spielmann, and F. Krausz, Nature (London) **433**, 596 (2005).
[9] B. Dromey, S. Kar, C. Bellei, D. C. Carroll, R. J. Clarke, J. S. Green, S. Kneip, K. Markey, S. R. Nagel, P. T. Simpson, L. Willingale, P. McKenna, D. Neely, Z. Najmudin, K. Krushelnick, P. A. Norreys, and M. Zepf, Phys. Rev. Lett. **99**, 085001 (2007).
[10] W. J. Brown, S. G. Anderson, C. P. J. Barty, S. M. Betts, R. Booth, J. K. Crane, R. R. Cross, D. N. Fittinghoff, D. J. Gibson, F. V. Hartemann, E. P. Hartouni, J. Kuba, G. P. Le Sage, D. R. Slaughter, A. M. Tremaine, A. J. Wootton, P. T. Springer, and J. B. Rosenzweig, Phys. Rev. ST Accel. Beams **7**, 060702 (2004).
[11] S. G. Rykovanov, C. G. R. Geddes, J.-L. Vay, C. B. Schroeder, E. Esarey, and W. P. Leemans, J. Phys. B **47**, 234013 (2014).
[12] H. Schwoerer, B. Liesfeld, H.-P. Schlenvoigt, K.-U. Amthor, and R. Sauerbrey, Phys. Rev. Lett. **96**, 014802 (2006).
[13] N. D. Powers, I. Ghebregziabher, G. Golovin, C. Liu, S. Chen, S. Banerjee, and D. P. Umstadter, Nat. Photonics **8**, 28 (2014).
[14] K. T. Phuoc, S. Corde, C. Thaury, V. Malka, A. Tafzi, J. P. Goddet, R. C. Shah, S. Sebban, and A. Rousse, Nat. Photonics **6**, 308 (2012).
[15] T. Tajima and J. M. Dawson, Phys. Rev. Lett. **43**, 267 (1979).
[16] E. Esarey, C. B. Schroeder, and W. P. Leemans, Rev. Mod. Phys. **81**, 1229 (2009).
[17] A. Pukhov and J. Meyer-ter Vehn, Appl. Phys. B Lasers Opt. **74**, 355 (2002).
[18] W. Lu, C. Huang, M. Zhou, W. B. Mori, and T. Katsouleas, Phys. Rev. Lett. **96**, 165002 (2006).
[19] S. Kneip *et al.*, Phys. Rev. Lett. **103**, 035002 (2009).
[20] H. T. Kim, K. H. Pae, H. J. Cha, I. J. Kim, T. J. Yu, J. H. Sung, S. K. Lee, T. M. Jeong, and J. Lee, Phys. Rev. Lett. **111**, 165002 (2013).
[21] X. Wang *et al.*, Nat. Commun. **4**, 1988 (2013).
[22] W. P. Leemans, A. J. Gonsalves, H.-S. Mao, K. Nakamura, C. Benedetti, C. B. Schroeder, C. Tóth, J. Daniels, D. E. Mittelberger, S. S. Bulanov, J.-L. Vay, C. G. R. Geddes, and E. Esarey, Phys. Rev. Lett. **113**, 245002 (2014).
[23] A. J. Gonsalves *et al.*, Phys. Rev. Lett. **122**, 084801 (2019).
[24] S. Wang, C. E. Clayton, B. E. Blue, E. S. Dodd, K. A. Marsh, W. B. Mori, C. Joshi, S. Lee, P. Muggli, T. Katsouleas, F. J. Decker, M. J. Hogan, R. H. Iverson, P. Raimondi, D. Walz, R. Siemann, and R. Assmann, Phys. Rev. Lett. **88**, 135004 (2002).
[25] A. Rousse, K. T. Phuoc, R. Shah, A. Pukhov, E. Lefebvre, V. Malka, S. Kiselev, F. Burgy, J.-P. Rousseau, D. Umstadter, and D. Hulin, Phys. Rev. Lett. **93**, 135005 (2004).
[26] S. Kneip *et al.*, Nat. Phys. **6**, 980 (2010).
[27] S. Corde, K. Ta Phuoc, G. Lambert, R. Fitour, V. Malka, A. Rousse, A. Beck, and E. Lefebvre, Rev. Mod. Phys. **85**, 1 (2013).
[28] J. M. Cole, J. C. Wood, N. C. Lopes, K. Poder, R. L. Abel, S. Alatabi, J. S. J. Bryant, A. Jin, S. Kneip, K. Mecseki, D. R. Symes, S. P. D. Mangles, and Z. Najmudin, Sci. Rep. **5**, 13244 (2015).
[29] M. S. Bloom, M. J. V. Streeter, S. Kneip, R. A. Bendoyro, O. Cheklov, J. M. Cole, A. Döpp, C. J. Hooker, J. Holloway, J. Jiang, N. C. Lopes, H. Nakamura, P. A. Norreys, P. P. Rajeev, D. R. Symes, J. Schreiber, J. C. Wood, M. Wing, Z. Najmudin, and S. P. D. Mangles, Phys. Rev. Accel. Beams **23**, 061301 (2020).
[30] K. T. Phuoc, S. Corde, R. Fitour, R. Shah, F. Albert, J.-P. Rousseau, F. Burgy, A. Rousse, V. Seredov, and A. Pukhov, Phys. Plasmas **15**, 073106 (2008).
[31] F. Albert, K. T. Phuoc, R. Shah, S. Corde, R. Fitour, A. Tafzi, F. Burgy, D. Douillet, T. Lefrou, and A. Rousse, Plasma Phys. Controlled Fusion **50**, 124008 (2008).
[32] K. T. Phuoc, R. Fitour, A. Tafzi, T. Garl, N. Artemiev, R. Shah, F. Albert, D. Boschetto, A. Rousse, D.-E. Kim, A. Pukhov, V. Seredov, and I. Kostyukov, Phys. Plasmas **14**, 080701 (2007).
[33] S. Kneip, C. McGuffey, F. Dollar, M. S. Bloom, V. Chvykov, G. Kalintchenko, K. Krushelnick, A. Maksimchuk, S. P. D. Mangles, T. Matsuoka, Z. Najmudin, C. A. J. Palmer, J. Schreiber, W. Schumaker, A. G. R. Thomas, and V. Yanovsky, Appl. Phys. Lett. **99**, 093701 (2011).
[34] S. Fourmaux, S. Corde, K. T. Phuoc, P. Lassonde, G. Lebrun, S. Payeur, F. Martin, S. Sebban, V. Malka, A. Rousse, and J. C. Kieffer, Opt. Lett. **36**, 2426 (2011).
[35] J. Wenz, S. Schleede, K. Khrennikov, M. Bech, P. Thibault, M. Heigoldt, F. Pfeiffer, and S. Karsch, Nat. Commun. **6**, 7568 (2015).
[36] J. M. Cole *et al.*, Proc. Natl. Acad. Sci. U.S.A. **115**, 6335 (2018).
[37] A. Döpp, L. Hehn, J. Götzfried, J. Wenz, M. Gilljohann, H. Ding, S. Schindler, F. Pfeiffer, and S. Karsch, Optica **5**, 199 (2018).
[38] A. E. Hussein *et al.*, Sci. Rep. **9**, 3249 (2019).
[39] J.-N. Gruse *et al.*, Nucl. Instrum. Methods Phys. Res., Sect. A **983**, 164369 (2020).
[40] D. Guénot, K. Svendsen, J. B. Svensson, H. Ekerfelt, A. Persson, O. Lundh, and E. Berrocal, Optica **7**, 131 (2020).
[41] A. Doherty, S. Fourmaux, R. Astolfo, A. amd Ziesche, J. Wood, O. Finlay, W. Stolp, D. Batey, I. Manke, F. Légaré, M. Boone, D. Symes, Z. Najmudin, M. Endrizzi, A. Olivo, and S. Cipiccia, Commun. Phys. **6**, 288 (2023).
[42] J. C. Wood *et al.*, Sci. Rep. **8**, 11010 (2018).
[43] F. Albert and A. G. R. Thomas, Plasma Phys. Controlled Fusion **58**, 103001 (2016).
[44] M. Šmíd, I. Gallardo González, H. Ekerfelt, J. Björklund Svensson, M. Hansson, J. C. Wood, A. Persson, S. P. D. Mangles, O. Lundh, and K. Falk, Rev. Sci. Instrum. **88**, 063102 (2017).

[45] B. Mahieu, N. Jourdain, K. Ta Phuoc, F. Dorchies, J. P. Goddet, A. Lifschitz, P. Renaudin, and L. Lecherbourg, Nat. Commun. **9**, 3276 (2018).

[46] B. Kettle *et al.*, Phys. Rev. Lett. **123**, 254801 (2019).

[47] B. Kettle *et al.*, Commun. Phys. **7**, 247 (2024).

[48] W. Lu, M. Tzoufras, C. Joshi, F. S. Tsung, W. B. Mori, J. Vieira, R. A. Fonseca, and L. O. Silva, Phys. Rev. ST Accel. Beams **10**, 061301 (2007).

[49] P. Foster, M. Streeter, J. Green, F. Cameron, C. Spindloe, G. Schumann, M. Tolley, R. Clarke, J. Collier, D. Neely, E. Divall, D. Neville, P. Rice, R. Bickerton, S. Blake, P. Holligan, P. Brumitt, and P. P. Rajeev, in *The European Conference on Lasers and Electro-Optics* (Optica Publishing Group, Washington DC, 2009), p. CG_P12.

[50] O. Kononenko, N. Lopes, J. Cole, C. Kamperidis, S. Mangles, Z. Najmudin, J. Osterhoff, K. Poder, D. Rusby, D. Symes, J. Warwick, J. Wood, and C. Palmer, Nucl. Instrum. Methods Phys. Res., Sect. A **829**, 125 (2016).

[51] R. Luo, G. R. Christian, M. P. Backhouse, N. C. Lopes, S. S. Alatabi, M. S. Bloom, M. Maier, and Z. Najmudin, High Power Laser Sci. Eng. **13**, e95 (2025).

[52] I. Glatt and O. Kafri, Opt. Lasers Eng. **8**, 277 (1988).

[53] B. Pollock *et al.*, in *Particle Accelerator Conference (PAC 09)* (JaCoW, Geneva, Switzerland, 2010), p. WE6RFP101.

[54] K. Põder, J. C. Wood, N. C. Lopes, J. M. Cole, S. Alatabi, M. P. Backhouse, P. S. Foster, A. J. Hughes, C. Kamperidis, O. Kononenko, S. P. D. Mangles, C. A. J. Palmer, D. Rusby, A. Sahai, G. Sarri, D. R. Symes, J. R. Warwick, and Z. Najmudin, Phys. Rev. Lett. **132**, 195001 (2024).

[55] K. A. Tanaka, T. Yabuuchi, T. Sato, R. Kodama, Y. Kitagawa, T. Takahashi, T. Ikeda, Y. Honda, and S. Okuda, Rev. Sci. Instrum. **76**, 013507 (2004).

[56] K. Zeil, S. D. Kraft, A. Jochmann, F. Kroll, W. Jahr, U. Schramm, L. Karsch, J. Pawelke, B. Hidding, and G. Pretzler, Rev. Sci. Instrum. **81**, 013307 (2010).

[57] E. Esarey, B. A. Shadwick, P. Catravas, and W. P. Leemans, Phys. Rev. E **65**, 056505 (2002).

[58] S. Fourmaux, S. Corde, K. T. Phuoc, P. M. Leguay, S. Payeur, P. Lassonde, S. Gnedyuk, G. Lebrun, C. Fourment, V. Malka, S. Sebban, A. Rousse, and J. C. Kieffer, New J. Phys. **13**, 033017 (2011).

[59] A. G. R. Thomas, Phys. Plasmas **17**, 056708 (2010).

[60] See Supplemental Material at http://link.aps.org/supplemental/10.1103/krsl-322s for further information on the x-ray spectral measurements and additional analysis of the simulation.

[61] M. J. V. Streeter, S. Kneip, M. S. Bloom, R. A. Bendoyro, O. Chekhlov, A. E. Dangor, A. Döpp, C. J. Hooker, J. Holloway, J. Jiang, N. C. Lopes, H. Nakamura, P. A. Norreys, C. A. J. Palmer, P. P. Rajeev, J. Schreiber, D. R. Symes, S. P. D. Wing, S. Mangles, and Z. Najmudin, Phys. Rev. Lett. **120**, 254801 (2018).

[62] C. D. Decker, W. B. Mori, K. Tzeng, and T. Katsouleas, Phys. Plasmas **3**, 2047 (1996).

[63] M. Heigoldt, A. Popp, K. Khrennikov, J. Wenz, S. W. Chou, S. Karsch, S. I. Bajlekov, S. M. Hooker, and B. Schmidt, Phys. Rev. ST Accel. Beams **18**, 121302 (2015).

[64] F. Fang, C. E. Clayton, K. A. Marsh, A. E. Pak, J. E. Ralph, N. C. Lopes, and C. Joshi, Plasma Phys. Controlled Fusion **51**, 024003 (2009).

[65] S. Kalmykov, S. A. Yi, V. Khudik, and G. Shvets, Phys. Rev. Lett. **103**, 135004 (2009).

[66] A. Sävert, S. P. D. Mangles, M. Schnell, E. Siminos, J. M. Cole, M. Leier, M. Reuter, M. B. Schwab, M. Möller, K. Poder, O. Jäckel, G. G. Paulus, C. Spielmann, S. Skupin, Z. Najmudin, and M. C. Kaluza, Phys. Rev. Lett. **115**, 055002 (2015).

[67] J. D. Jackson, *Classical Electrodynamics* (Wiley, New York, 1999), 3rd ed.

[68] A. G. Khachatryan, A. Irman, F. A. van Goor, and K.-J. Boller, Phys. Rev. ST Accel. Beams **10**, 121301 (2007).

[69] S. Cipiccia *et al.*, Nat. Phys. **7**, 867 (2011).

[70] W. Yan, L. Chen, D. Li, L. Zhang, N. a. M. Hafz, J. Dunn, Y. Ma, K. Huang, L. Su, M. Chen, Z. Sheng, and J. Zhang, Proc. Natl. Acad. Sci. U.S.A. **111**, 5825 (2014).

[71] S. Fourmaux, K. Otani, A. Saraf, S. MacLean, M. J. Wesolowski, P. S. Babyn, E. Hallin, A. Krol, and J. C. Kieffer, in *Relativistic Plasma Waves and Particle Beams as Coherent and Incoherent Radiation Sources*, edited by D. A. Jaroszynski, International Society for Optics and Photonics (SPIE, Bellingham, Washington, USA, 2015), Vol. 9509, p. 950907, 10.1117/12.2087603.

[72] A. Döpp, B. Mahieu, A. Lifschitz, C. Thaury, A. Doche, E. Guillaume, G. Grittani, O. Lundh, M. Hansson, J. Gautier, M. Kozlova, J.-P. Goddet, P. Rousseau, A. Tafzi, V. Malka, A. Rousse, S. Corde, and K. Ta Phuoc, Light Sci. Appl. **6**, e17086 (2017).

[73] F. Albert, N. Lemos, J. L. Shaw, B. B. Pollock, C. Goyon, W. Schumaker, A. M. Saunders, K. A. Marsh, A. Pak, J. E. Ralph, J. L. Martins, L. D. Amorim, R. W. Falcone, S. H. Glenzer, J. D. Moody, and C. Joshi, Phys. Rev. Lett. **118**, 134801 (2017).

[74] C. F. Dong, T. Z. Zhao, K. Behm, P. G. Cummings, J. Nees, A. Maksimchuk, V. Yanovsky, K. Krushelnick, and A. G. R. Thomas, Phys. Rev. Accel. Beams **21**, 041303 (2018).

[75] R. Rakowski, P. Zhang, K. Jensen, B. Kettle, T. Kawamoto, S. Banerjee, C. Fruhling, G. Golovin, D. Haden, M. S. Robinson, D. Umstadter, B. A. Shadwick, and M. Fuchs, Sci. Rep. **12**, 10855 (2022).

[76] R. Lehe, M. Kirchen, I. A. Andriyash, B. B. Godfrey, and J.-L. Vay, Comput. Phys. Commun. **203**, 66 (2016).

[77] S. Y. Kalmykov, A. Beck, S. A. Yi, V. N. Khudik, M. C. Downer, E. Lefebvre, B. A. Shadwick, and D. P. Umstadter, Phys. Plasmas **18**, 056704 (2011).

[78] F. S. Tsung, C. Ren, L. O. Silva, W. B. Mori, and T. Katsouleas, Proc. Natl. Acad. Sci. U.S.A. **99**, 29 (2002).

[79] J. Faure, Y. Glinec, J. J. Santos, F. Ewald, J.-P. Rousseau, S. Kiselev, A. Pukhov, T. Hosokai, and V. Malka, Phys. Rev. Lett. **95**, 205003 (2005).

[80] J. Götzfried, A. Döpp, M. F. Gilljohann, F. M. Foerster, H. Ding, S. Schindler, G. Schilling, A. Buck, L. Veisz, and S. Karsch, Phys. Rev. X **10**, 041015 (2020).

[81] Y. Ma *et al.*, Phys. Rev. X **15**, 031062 (2025).

[82] S. Kneip, S. R. Nagel, C. Bellei, N. Bourgeois, A. E. Dangor, A. Gopal, R. Heathcote, S. P. D. Mangles, J. R. Marquès, A. Maksimchuk, P. M. Nilson, K. T. Phuoc, S. Reed, M. Tzoufras, F. S. Tsung, L. Willingale, W. B. Mori, A. Rousse, K. Krushelnick, and Z. Najmudin, Phys. Rev. Lett. **100**, 105006 (2008).